

MASS: MoErging through Adaptive Subspace Selection

Donato Crisostomi* Alessandro Zirilli* Antonio Andrea Gargiulo Maria Sofia Bucarelli
Simone Scardapane Fabrizio Silvestri Iacopo Masi Emanuele Rodolà
Sapienza University of Rome

{crisostomi, gargiulo, masi, rodola}@di.uniroma1.it zirilli.1967394@studenti.uniroma1.it
simone.scardapane@uniroma1.it {bucarelli, fsilvestri}@diag.uniroma1.it

Abstract

Model merging has recently emerged as a lightweight alternative to ensembling, combining multiple fine-tuned models into a single set of parameters with no additional training overhead. Yet, existing merging methods fall short of matching the full accuracy of separately fine-tuned endpoints. We present MASS (MoErging through Adaptive Subspace Selection), a new approach that closes this gap by unifying multiple fine-tuned models while retaining near state-of-the-art performance across tasks. Building on the low-rank decomposition of per-task updates, MASS stores only the most salient singular components for each task and merges them into a shared model. At inference time, a non-parametric, data-free router identifies which subspace (or combination thereof) best explains an input’s intermediate features and activates the corresponding task-specific block. This procedure is fully training-free and introduces only a two-pass inference overhead plus a $\sim 2\times$ storage factor compared to a single pretrained model, irrespective of the number of tasks. We evaluate MASS on CLIP-based image classification using ViT-B-16, ViT-B-32 and ViT-L-14 for benchmarks of 8, 14 and 20 tasks respectively, establishing a new state-of-the-art. Most notably, MASS recovers up to $\sim 98\%$ of the average accuracy of individual fine-tuned models, making it a practical alternative to ensembling at a fraction of the storage cost.

1. Introduction

In the early days of deep learning, the default practice was to train models entirely from scratch. Later, with the rise of massive pretrained networks, research pivoted toward fine-tuning these backbones for specialized tasks [17, 32, 52, 60, 73]. Nowadays, thanks to the abundance of publicly available fine-tuned models in repositories like

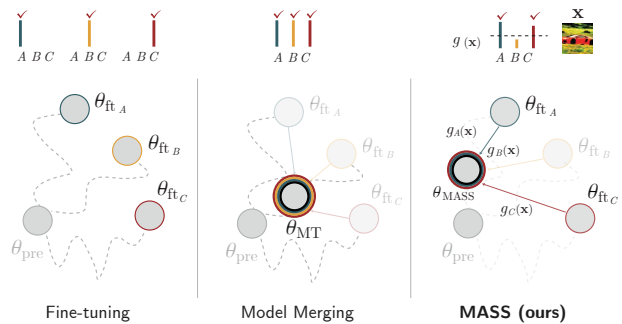


Figure 1. (left) Fine-tuning holds three separate models on different tasks A, B and C. (middle) Model merging produces a single model incorporating task vectors $\{A, B, C\}$ using a constant function of the input. (right) MASS stores the pretrained model θ_{pre} and the orthogonalized task singular vectors V_{\perp}^{\top} across tasks. At test time, MASS adaptively performs merging using a routing mechanism that chooses appropriate task vectors for the input \mathbf{x} , using a thresholded gating function $g(\mathbf{x})$. The gate is the residual between the activations of \mathbf{x} and their projections onto the span of the right singular vectors V_{\perp} .

HuggingFace¹, we are witnessing a new shift. This time, the focus is on *no-tuning* methods that can simultaneously leverage both the pretrained foundation and the diverse range of existing fine-tuned endpoints. Among these, *model merging* [1, 2, 13, 14, 25, 34, 54, 69, 74, 76] has gained significant attention. By combining multiple fine-tuned models into a single parameter set, merging offers a practical, lightweight alternative to ensembling.

A particularly effective application of model merging is the aggregation of models fine-tuned for different tasks from a shared backbone. Techniques such as Task Arithmetic [34] and its extensions [2, 14, 33, 48, 65, 69, 74] treat each task-specific update as a flat *task vector* – the difference between the pre-trained and fine-tuned weights

¹<https://huggingface.co/docs/hub/models-the-hub>

– and obtain a multitask model by summing these vectors, often with simple rescaling. More recent work [15, 25] has shown that preserving the layer-wise structure of fine-tuned weight updates leads to better performance. Instead of treating task updates as flat vectors, methods like `Task Singular Vectors (TSV)` [25] leverage the inherent matrix structure of these updates. TSV, in particular, finds that the per-layer delta matrices exhibit a strong low-rank structure, where a small number of singular vectors per task retain most of the classification accuracy.

Despite these advances, structured merging methods remain limited by a key constraint: their aggregation step is predetermined and remains unchanged regardless of the input. This rigidity leads to suboptimal performance, and some tasks suffer disproportionately. For instance, TSV reports a $\sim 60\%$ accuracy drop for the worst-performing task compared to its fine-tuned endpoint.

In this work, we propose coupling the aggregation capabilities of structured model merging approaches with the adaptivity of Mixture of Experts (MoE) [19, 20, 22, 53] methods, yielding a new state-of-the-art model MoErging method [70]. Capitalizing on task singular vectors, MASS dynamically selects the most relevant tasks by employing an adaptive routing mechanism that conditions the merging process on the input itself, as shown in Fig. 1.

Yet, existing routing techniques are ill-suited for model merging, as they typically require task-specific data for retrieval-based selection or even training [40, 51, 63]. This reliance makes them incompatible with the merging setting, where models are often uploaded without any associated data. To overcome this, we couple MASS with a novel weight-space router that identifies the most relevant task subspaces – defined by their task singular vectors – without requiring any data or additional fine-tuning. By selectively integrating these subspaces into the pre-trained model, MASS enables a fully training-free and data-free merging process, ensuring broad applicability.

We evaluate MASS on ViT-B-32, ViT-B-16, and ViT-L-14 architectures for 8, 14, and 20 tasks, showing a significant improvement over existing model merging techniques. For a modest increase in computational cost ($\sim 2\times$ forward passes) and storage ($\sim 2\times$ parameter footprint regardless of number of tasks), our method achieves an average accuracy within 5% of independently fine-tuned models across all scales. When used in a batched setting, MASS completely bridges the performance gap for 8 benchmarks out of 9, reducing the accuracy drop to below 1%.

Wrapping up, our contribution is three-fold:

- We propose MASS, a MoErging method that integrates routing capabilities into singular vector-based merging.
- We couple it with a novel projection-based router that requires no task data or tuning, making it specifically suited for MoErging.

- We extensively evaluate our approach, establishing a new state-of-the-art in the process.

We release our code, checkpoints, and all relevant logs for research purposes².

2. Background

In this section, we introduce key concepts for understanding our approach.

2.1. Task Vectors

`Task Arithmetic (TA)` [34] defines task vectors capturing the specific differences in model weights for individual tasks. Formally, the weights θ_{MT} of a multi-task model for T tasks are computed by aggregating the task-specific weight differences, or task vectors, as follows:

$$\theta_{\text{MT}} = \theta_{\text{pre}} + \alpha \sum_{i=1}^T \tau_i, \quad (1)$$

where θ_{pre} is the set of pretrained model weights, α is a scaling factor, and $\tau_i = \theta_{\text{ft}_i} - \theta_{\text{pre}}$ is the task vector for task i , with θ_{ft_i} being the fine-tuned weights for the task. Following Gargiulo et al. [25], however, we consider these operations at the layer level. From a layer-wise perspective, Eq. (1) can be rewritten as

$$\theta_{\text{MT}}^{(\ell)} = \theta_{\text{pre}}^{(\ell)} + \alpha \sum_{i=1}^T \Delta_i^{(\ell)}, \quad (2)$$

where $\theta_{\text{pre}}^{(\ell)}$ encodes the pretrained weights for layer ℓ , and $\Delta_i^{(\ell)} = \theta_{\text{ft}_i}^{(\ell)} - \theta_{\text{pre}}^{(\ell)}$ is the task-specific weight difference for task i at layer ℓ . When layer ℓ has a matrix structure, its corresponding $\Delta_i^{(\ell)}$ is called the *per-layer task matrix* for task i . The layer index will be omitted for brevity.

2.2. Task Singular Vectors

Given a task i , Gargiulo et al. [25] consider the SVD of the corresponding task matrices Δ_i on a generic layer:

$$\Delta_i = U_i \Sigma_i V_i^\top.$$

They then truncate the decomposition to rank k obtaining the truncated left and right singular vectors $\tilde{U}_i = U_{i[:,1:k]}$ and $\tilde{V}_i = V_{i[1:k]}$ and the truncated matrix of the singular values $\tilde{\Sigma}_i = \Sigma_{i[1:k]}$.

By defining $U = [\tilde{U}_1 \dots \tilde{U}_T]$ as the column-wise concatenation of the top- k left TSVs, $V = [\tilde{V}_1 \dots \tilde{V}_T]$ as the concatenation of the top- k right TSVs and $\tilde{\Sigma}$ as a block diagonal matrix with $\{\tilde{\Sigma}_i\}_{i=1}^T$ along its diagonal, TSV-M [25] replaces the sum of the layer-wise Δ 's in Eq. (2) with

$$\hat{\Delta} = U_\perp \Sigma V_\perp^\top, \quad (3)$$

²github.com/crisostomi/mass

where U_{\perp} and V_{\perp}^{\top} are orthogonalized to reduce inter-task interference. In practice, this is equivalent to summing the top- k rank-one matrices for each task, with an added orthogonalization step to prevent singular vectors belonging to different tasks from interfering. The full procedure is detailed in Algorithm 1 (lines 10–20).

3. Approach

Our approach is best understood as a pre-processing step followed by an inference-time step. The former consists of a one-time merging procedure to obtain an encoder model θ_{MT} , as detailed in Algorithm 1. We refer to this as the ‘fixed’ merging step, as it is performed only once and remains independent of the input. During inference, θ_{MT} is used in a dynamic process, outlined in Algorithm 2, consisting of 4 steps:

- (i) **First pass:** forward the input through θ_{MT} ;
- (ii) **Routing:** project the input onto each task subspace at a chosen layer and select those with the lowest projection error;
- (iii) **Adaptive merge:** merge the selected task subspaces into Δ_{ada} ;
- (iv) **Second pass:** classify the input using $\theta_{\text{pre}} + \alpha \Delta_{\text{ada}}$.

Algorithm 1 Fixed Merging Step

Require: Pretrained model weights θ_{pre} , task-specific updates $\{\Delta_i\}_{i=1}^T$, user-specified threshold ε

Ensure: Fixed merged model weights θ_{MT}

- 1: **Accounting for redundant directions** (Sec. 3.2.2)
 - 2: $\mathcal{M} = \{\}$
 - 3: **for** $i = 1, \dots, T$ **do**
 - 4: $\delta_i \leftarrow \text{vec}(\Delta_i)$
 - 5: **if** $\max_{\{j \in \mathcal{M}\}} \text{sim}(\delta_i, \delta_j) < \varepsilon$ **then**
 - 6: $\mathcal{M} \leftarrow \mathcal{M} \cup \{i\}$
 - 7: **end if**
 - 8: **end for**
 - 9: **Merging step using** TSV-M [25] **on the** $\{\Delta_i\}_{i \in \mathcal{M}}$
 - 10: **for** $i \in \mathcal{M}$ **do**
 - 11: $\Delta_i = U_i \Sigma_i V_i^{\top}$
 - 12: $\tilde{U}_i \leftarrow U_{i[:,1:k]}$, $\tilde{\Sigma}_i \leftarrow \Sigma_{i[1:k,1:k]}$, $\tilde{V}_i \leftarrow V_{i[:,1:k]}$
 - 13: **end for**
 - 14: $U \leftarrow [\tilde{U}_1 | \tilde{U}_2 | \dots | \tilde{U}_T]$
 - 15: $\Sigma \leftarrow \text{block_diag}(\tilde{\Sigma}_1, \tilde{\Sigma}_2, \dots, \tilde{\Sigma}_T)$
 - 16: $V \leftarrow [\tilde{V}_1 | \tilde{V}_2 | \dots | \tilde{V}_T]$
 - 17: $U_{\perp} \leftarrow \text{orthogonalize}(U)$
 - 18: $V_{\perp} \leftarrow \text{orthogonalize}(V)$
 - 19: $\hat{\Delta} \leftarrow U_{\perp} \Sigma V_{\perp}^{\top}$
 - 20: $\theta_{\text{MT}} \leftarrow \theta_{\text{pre}} + \alpha \hat{\Delta}$
 - 21: **return** θ_{MT}
-

3.1. Fixed merging

We begin with a one-time merging step to produce a model capable of task discrimination. This model provides the intermediate activations used by the router in the first pass. For this, we use TSV-M [25] due to its subspace-aware aggregation. While one could use the base model instead, Tab. 3 shows it performs worse at distinguishing tasks.

3.2. Integrating routing

We extend the aggregation step in Eq. (1) to include a routing mechanism. Given an input \mathbf{x} , the merged model can be adaptively determined by

$$\theta_{\text{MT}} = \theta_{\text{pre}} + \alpha \sum_{i=1}^T \mathbb{1}_{[g_i(\mathbf{x})=1]}(\mathbf{x}) \tau_i, \quad (4)$$

where $g_i(\mathbf{x})$ is a per-task gating function that only selects tasks meeting a criterion. Replacing the naive aggregation with task singular vector-based aggregation yields a merged model described by the following equation

$$\theta_{\text{MT}} = \theta_{\text{pre}} + \alpha \sum_{i=1}^T \mathbb{1}_{[g_i(\mathbf{x})=1]}(\mathbf{x}) \sum_{j=1}^k \sigma_j^i u_j^i v_j^{i\top}. \quad (5)$$

In other words, $g_i(\mathbf{x})$ adaptively selects which task subspaces to activate, and subsequently merge, depending on the input at hand. Traditionally, however, routers require either task-specific data for non-parametric procedures such as nearest-neighbor-based routing or both data and training for parametric routers (Tab. 3). This contrasts with the usual merging scenario that does not assume access to the data used to train the endpoint models – as these could be, in principle, downloaded from any public model repository. We therefore introduce a completely *data-* and *tuning-free* approach.

Router	Requires	
	Training	Data
nn	×	✓
mlp	✓	✓
ours	×	×

Table 1. Routing strategies and requirements.

3.2.1. Projection-based routing

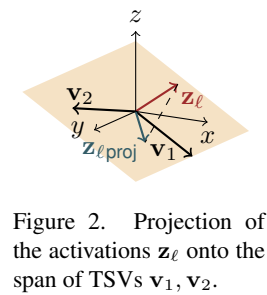


Figure 2. Projection of the activations \mathbf{z}_{ℓ} onto the span of TSVs $\mathbf{v}_1, \mathbf{v}_2$.

Given an input intermediate representation \mathbf{z}_{ℓ} for a pre-determined layer ℓ , we want to identify which task subspace (or set of subspaces) is the most relevant. Concretely, one way to do this is to compute the Euclidean residual of \mathbf{z}_{ℓ} after projecting onto $\text{span}(V_i^{(\ell)})$:

$$r_i = \|\mathbf{z}_{\ell} - \text{Proj}_{V_i^{(\ell)}}(\mathbf{z}_{\ell})\|_2, \quad (6)$$

where $\text{Proj}_{V_i^{(\ell)}}(\mathbf{z}_\ell) = V_i^{(\ell)}(V_i^{(\ell)})^\top \mathbf{z}_\ell$ is the optimal L_2 projector. At this point, the additive inverse of the residuals may be normalized through a softmax to obtain the coefficients. The router then picks those exceeding a predetermined threshold η , obtained by evaluating its behavior on the validation set, limiting the selection to the top- k when more tasks surpass it. For details regarding the choice of the layer used to compute the residual, see Sec. 4.1.

Algorithm 2 Adaptive Merging Step

Require: Pretrained model weights θ_{pre} , task-specific updates $\{\Delta_i\}_{i=1}^T$, fixed merged model θ_{MT} , top- k parameter k , threshold η , task-specific classification heads $\{h_i\}_{i=1}^T$, sample \mathbf{x}




Ensure: Predicted class c^*

```

1:  $\mathbf{z}_\ell \leftarrow \text{ForwardPass}(\theta_{\text{MT}}, \mathbf{x})$  # first pass
2: for  $i = 1, \dots, T$  do
3:    $r_i \leftarrow \|\mathbf{z}_\ell - V_i V_i^\top \mathbf{z}_\ell\|_2$  # residual as Eq. (6)
4: end for
5:  $w \leftarrow \text{softmax}(-r)$ 
6:  $\Omega \leftarrow \{i : w_i \geq \eta\}$  # Select tasks above threshold
7:  $\Omega \leftarrow \text{TopK}(\Omega, w, k)$  # Keep only top- $k$  weighted tasks
8: Merge selected subspaces
9:  $\Delta_{\text{ada}} \leftarrow \sum_{i \in \Omega} U_i \Sigma_i V_i^\top$ 
10: Compute adaptive model:  $\theta_{\text{MASS}} \leftarrow \theta_{\text{pre}} + \alpha \Delta_{\text{ada}}$ 
11: Classification procedure
12:  $\mathbf{z}_{L-1} \leftarrow \text{ForwardPass}(\theta_{\text{MASS}}, \mathbf{x})$  # Compute shared representation
13:  $\mathbf{z}_i \leftarrow h_i(\mathbf{z}_{L-1})$  # Evaluate each head
14:  $(i^*, c^*) \leftarrow \arg \max_{(i,c) \in \Omega \times \{1, \dots, C_i\}} z_i[c]$  # Highest logit across heads
15: return  $c^*$ 

```

3.2.2. Accounting for redundant directions

In order for projection-based routing to be effective, no task(s) should overshadow the others. Consider, for example, three tasks: MNIST , EMNIST , and KMNISt . Being trained on very similar datasets covering the same classes, Δ_{MN} and Δ_{EMN} share a large portion of their right-singular directions:

$$\text{span}(V_{\text{MN}}^{(\ell)}) \approx \text{span}(V_{\text{EMN}}^{(\ell)}),$$

while KMNISt has some distinct directions $V_{\text{KM}}^{(\ell)}$ capturing more Japanese *kana*-like shapes. However, all three tasks may agree on certain generic “black background, white glyph” features. Because MNIST and EMNIST partially *reinforce* these directions (they both include them), the *union* of their subspaces can appear “wider” or more dominant in that region of feature space. Consequently, for many test samples \mathbf{z}_ℓ with black backgrounds and centered shapes:

$$\|\mathbf{z}_\ell - \text{Proj}_{V_{\text{MN}} \cup V_{\text{EMN}}}(\mathbf{z}_\ell)\|_2 < \|\mathbf{z}_\ell - \text{Proj}_{V_{\text{KM}}}(\mathbf{z}_\ell)\|_2.$$

Hence, the router sees a smaller residual for MNIST/EMNIST, declaring those tasks more suitable even if the glyph belongs to KMNISt.

During the fixed merging step, instead of aggregating all task matrices, we only keep those that are *sufficiently distinct*. We first select a single task matrix as the initial element of the merge set. Then, for each remaining task matrix, we determine whether to include it based on its similarity to the matrices already in the set. A task matrix is added only if its similarity to all previously accepted matrices remains below a predefined threshold. Formally, let $\{\Delta_{a_1}, \dots, \Delta_{a_r}\}$ be the set of accepted updates at a given layer. When evaluating a new task update Δ_i , we flatten it as $\delta_i = \text{vec}(\Delta_i)$ and compute its cosine similarity $\text{sim}(\delta_i, \delta_{a_m})$ with each previously accepted update δ_{a_m} . If

$$\max_{1 \leq m \leq r} \text{sim}(\delta_i, \delta_{a_m}) > \varepsilon,$$

where ε is a user-specified threshold (e.g. $\varepsilon = 0.3$), we discard Δ_i and do *not* merge it; else we accept it. This ensures that highly similar task subspaces do not overshadow less common ones. This procedure is performed before the merging, see lines 2–8 of Algorithm 1.

3.3. Adaptive Merging and Inference

With the router having selected a subset Ω of relevant tasks, we merge their subspaces via TSV-M [25] into a single model θ_{MASS} . Crucially, unlike standard model merging – which assumes an oracle provides the correct task head at inference – we do *not* know the task in advance. Instead, after obtaining the shared representation $\mathbf{z}_{L-1} \in \mathbb{R}^d$ from θ_{MASS} , we run each head $h_i : \mathbb{R}^d \rightarrow \mathbb{R}^{C_i}$ for every selected task $i \in \Omega$:

$$\mathbf{z}_i = h_i(\mathbf{z}_{L-1}), \quad \mathbf{z}_i \in \mathbb{R}^{C_i}.$$

We then pick the highest logit among all heads in Ω . Formally:

$$(i^*, c^*) = \arg \max_{(i,c) \in \Omega \times \{1, \dots, C_i\}} z_i[c].$$

In other words, we identify which head i^* is most “confident” and select its predicted class c^* . This procedure thus covers the *unknown-task* scenario, allowing the model to determine both head and label space on a per-input basis.

4. Experiments

Models and baselines We conduct our experiments on three versions of the CLIP [52] model, each equipped with a different ViT [18] visual encoder: ViT-B-32, ViT-B-16, and ViT-L-14. As baselines, we compare against multiple training-free merging strategies, notably weight averaging, Task Arithmetic [34], and Consensus Merging [65]. For additional context,

Method		ViT-B-32			ViT-B-16			ViT-L-14		
		8 tasks	14 tasks	20 tasks	8 tasks	14 tasks	20 tasks	8 tasks	14 tasks	20 tasks
Base	Zeroshot	48.2 _(53.5)	57.2 _(63.6)	56.1 _(62.4)	55.3 _(59.3)	61.2 _(66.1)	59.7 _(64.5)	64.7 _(68.0)	68.2 _(72.1)	65.2 _(68.9)
	Finetuned	92.8 _(1.00)	90.8 _(1.00)	91.3 _(1.00)	94.6 _(1.00)	92.7 _(1.00)	93.1 _(1.00)	95.8 _(1.00)	94.2 _(1.00)	94.7 _(1.00)
Fixed	Weight Averaging	66.3 _(72.1)	64.3 _(71.1)	61.0 _(67.5)	72.2 _(76.6)	69.4 _(74.8)	65.3 _(70.3)	79.5 _(83.1)	76.7 _(81.1)	71.6 _(75.6)
	Task Arithmetic [34]	70.7 _(76.5)	65.3 _(72.0)	60.5 _(66.7)	75.4 _(79.5)	70.5 _(75.8)	65.7 _(70.7)	84.9 _(88.6)	79.4 _(83.9)	74.0 _(78.0)
	Consensus TA [65]	75.0 _(80.8)	70.3 _(77.3)	65.4 _(71.9)	79.3 _(83.8)	74.3 _(79.9)	69.7 _(74.9)	86.3 _(90.0)	82.2 _(86.9)	79.0 _(83.2)
	TSV-M [25]	85.8 _(92.3)	80.0 _(87.8)	77.0 _(84.2)	89.0 _(93.9)	84.5 _(91.0)	80.5 _(86.4)	92.9 _(96.9)	89.1 _(94.4)	87.7 _(92.5)
	Iso-C [15]	86.3 _(92.9)	80.3 _(88.1)	75.5 _(82.5)	90.6 _(95.6)	84.8 _(91.1)	79.6 _(85.4)	94.2 _(98.3)	89.3 _(94.5)	87.6 _(92.2)
	Iso-CTS [15]	86.2 _(92.8)	81.7 _(89.7)	78.1 _(85.5)	91.1 _(96.1)	86.4 _(92.8)	82.4 _(88.4)	94.7 _(98.8)	91.0 _(96.3)	90.1 _(94.9)
MoE	MASS	90.6_(97.6)	86.8_(95.5)	84.4_(92.5)	93.2_(98.5)	90.2_(97.3)	85.3_(91.9)	94.6_(98.7)	91.4_(97.0)	90.6_(95.7)

Table 2. Average absolute accuracy results on model merging benchmarks; subscript (in parentheses) is the normalized average accuracy.

zero-shot performance serves as a null reference point, and the mean accuracy of individually fine-tuned models marks the upper bound on achievable performance.

Benchmark We evaluate on three collections of tasks, containing 8, 14, and 20 tasks respectively. The latter is the most extensive setup considered in [15, 25, 65]. The 8-task benchmark, introduced in [34], comprises the following datasets: Cars [37], DTD [9], EuroSAT [30], GTSRB [56], MNIST [39], RESISC45 [7], SUN397 [68], and SVHN [46]. Moving to 14 tasks, we add CIFAR100 [38], STL10 [11], Flowers102 [47], OxfordIIITPet [50], PCAM [64], and FER2013 [27]. The 20-task suite further includes EMNIST [12], CIFAR10 [38], Food101 [5], FashionMNIST [67], RenderedSST2 [55], and KMNIST [10]. We quantify results using both average absolute accuracy and average normalized accuracy.

MoErging results Tab. 2 reports the average absolute accuracy and the corresponding normalized accuracy (subscript, also in percentage) for each method, model size, and number of tasks. We first note that MASS sets a new state of the art across all benchmarks: it consistently surpasses both classic methods like Task Arithmetic [34] and Consensus TA [65], as well as more recent approaches such as Iso-C and Iso-CTS [15].

Focusing on the largest (20-task) benchmark, we see that MASS outperforms the fixed baseline TSV-M by +7.4% absolute accuracy with ViT-B-32, +4.8% with ViT-B-16, and +2.9% with ViT-L-14. Normalized accuracies (in parentheses) confirm these gains, indicating that MASS preserves a far higher fraction of each original fine-tuned model’s performance. Interestingly, the largest accuracy gaps appear on the smaller encoders (ViT-B-32 and ViT-B-16) with many tasks, suggesting that our router-based strategy more effectively mitigates task interference

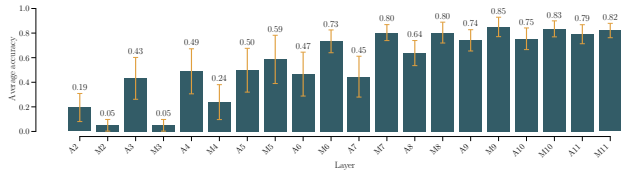
where capacity is at a premium. Meanwhile, on the ViT-L-14, MASS still improves upon the baselines, albeit by a smaller margin – possibly suggesting that larger backbones are more robust to interference in the first place.

We illustrate a per-task breakdown of these improvements in Fig. 4 for the 20-task setting; the corresponding plots for 8 and 14 tasks appear, respectively, in Fig. 9 and Fig. 10 in the supplementary material. We see here that MASS not only raises the overall average but also consistently preserves a high percentage of each task’s individual accuracy: in the 8-task benchmarks, MASS retains at least 94% of the fine-tuned accuracy for every single task. For the 14-task setting, each task individually maintains at least 83% of its original accuracy. Even with 20 tasks, MASS still reduces large drops, preserving above 80% for 19 tasks in ViT-B-32 and ViT-B-16, and 18 for ViT-L-14. Thus, while Tab. 2 shows the average improvements, Fig. 4 confirms that these gains extend consistently across all tasks, rather than masking a few poor-performing outliers.

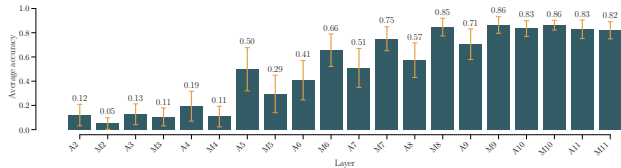
We also compare MASS with TwinMerging [40] under the 8-task benchmark on ViT-B-32, the only scenario for which their paper provides final results. Although the repository does not include the evaluation code necessary to replicate other setups, we find that MASS achieves 97.6% normalized accuracy in this shared setting, exceeding the 95.3% reported for TwinMerging. Notably, the latter assumes oracle knowledge of the correct classification head, whereas MASS selects both the merged experts and the output space at inference time. Despite operating in a more general setting, MASS still reaches a higher accuracy.

4.1. Choosing a routing layer

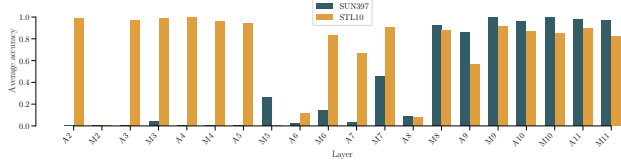
We now investigate the effect of routing layer selection on task accuracy. Figure 3 shows the task prediction accuracy obtained by routing at different layers for ViT-B-32 and ViT-B-16 architectures. Interestingly, the best layer



(a) Averaged across all tasks for a ViT-B-32.



(b) Averaged across all tasks for a ViT-B-16.



(c) Focusing on SUN397 and STL10 for a ViT-B-32.

Figure 3. Per-layer task accuracies for ViT-B-32 on the 20-task benchmark. Layers starting with ‘A’ indicate attention layers, while those starting with ‘M’ refer to MLPs.

is consistent across architectures, with ViT-B-32 and ViT-B-16 both achieving peak performance at layer 9, and MLP layers exhibiting slightly better performance than the self-attention layers.

It is immediate to see, however, that the best layer varies significantly across tasks. In fact, the error bars show some layers to have a standard deviation of up to 40% in accuracy across tasks. This can be better appreciated by looking at Figure 3c, where we can see the per-layer task accuracies on STL10 and SUN397 for a ViT-B-32. While both tasks can be accurately predicted with the best chosen layer $\ell = 9$, the former shows a marked improvement in accuracy when routing at earlier layers $\ell = 3, 4, 5$, while the latter benefits from routing at later layers $\ell = 9, 10, 11$ and results in poor performance in the earlier ones. This suggests that the best routing layer is task-dependent, and may encourage further research on adaptive ways to determine it. We report an analogous analysis for the ViT-L-14 model in the supplementary materials.

4.2. Comparison with other routers

We now compare our router with two common routing strategies, each with its own benefits and drawbacks in terms of accuracy, data, and computation requirements.

Nearest Neighbor to task data (NN). In this approach, we first construct a small *support set* of representative ex-

MASS	ViT-B-32			ViT-B-16		
	8 tasks	14 tasks	20 tasks	8 tasks	14 tasks	20 tasks
+						
nn	94.5	91.3	91.3	93.5	91.7	86.5
mlp	98.9	98.2	96.4	98.9	98.4	95.0
proj _{PRE}	96.2	90.4	76.7	97.9	97.3	81.1
proj _{TSV-M}	97.6	95.5	92.5	98.5	97.3	91.9

Table 3. Average normalized accuracy for different routers.

amples from each task’s validation data. For each test sample, we compare its intermediate representation \mathbf{z}_ℓ to the stored representations of all support examples. Formally, we compute the cosine similarity to each support sample and take the nearest neighbor among all tasks, inferring the task identity from whichever task that support sample belongs to. This method requires no additional parameters but does assume access to—and storage for—a curated batch of validation embeddings per task.

Learnable router (MLP). Our third strategy learns an MLP over the union of validation sets from all tasks, with each example labeled by its originating task. Concretely, after extracting \mathbf{z}_ℓ for each validation example, we train an MLP f_θ to output a probability distribution over the tasks. The latter is learned via cross-entropy minimization on the union of all tasks’ validation data. Architectural details are provided in the supplementary materials.

Results Tab. 3 shows the average normalized accuracy obtained by MASS when varying routing strategy. The NN approach, which stores and compares with a small validation set from each task, generally performs well but remains slightly below our best results. The MLP router achieves the highest accuracy overall, but it relies on a labeled validation set for training—a requirement that contradicts the core premise of merging methods, where access to original task data is often unavailable. This dependency makes the MLP less broadly applicable in realistic scenarios, such as when downloading fine-tuned models from public hubs without any accompanying data. Focusing on the projection-based router (proj), we observe that starting from the TSV-M model (proj_{TSV-M}) outperforms routing from the pretrained backbone (proj_{PRE}). This gap underscores the core key insight behind our method: TSV-M arranges each task’s top singular vectors into distinct, largely orthogonal subspaces, all contained in the final merged model. Consequently, proj_{TSV-M} only needs to measure how well each subspace reconstructs the activations—“finding back” the subspace that was originally embedded for each task. In other words, once TSV-M has embedded each task’s directions into a single model, a residual-based projection (cf.

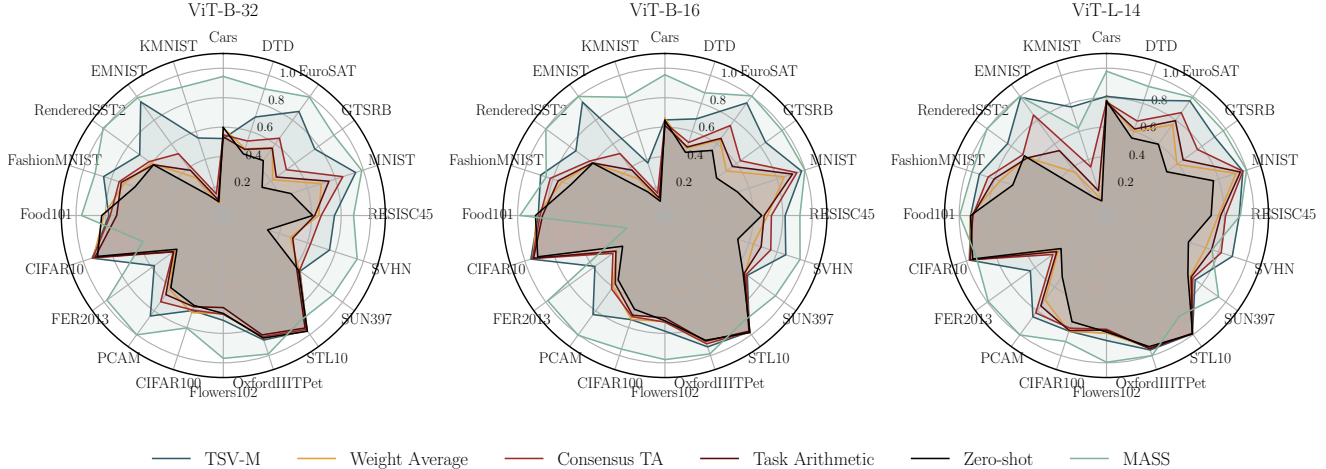


Figure 4. Normalized task accuracies over models ViT-B-32, ViT-B-16 and ViT-L-14 for the 20 tasks benchmark.

Eq. (6)) is enough to pinpoint the correct subspace, requiring no labels or additional training.

4.3. Interpreting task singular vectors

Finally, we attempt to interpret the task singular vectors that are used for routing in MASS. Notably, prior work suggests that mid-layer embeddings in CLIP-like models preserve semantic content, implying that routing at this layer hinges on meaningful features. To validate this, we interpret TSVs using the TEXTSPAN algorithm [3, 24]. The latter iteratively identifies and removes the most influential text directions, revealing which concepts best explain how the model’s weight changes affect its representation.

Our results, illustrated in Figure 5 confirm that TSVs capture meaningful and interpretable visual-language associations. For example, the singular vectors associated with the Cars dataset [37] strongly activate the description “IMAGE OF A CAR”, whereas those for the DTD dataset [9] align closely with the phrase “CLOSE-UP OF A TEXTURED MESH”. Interestingly, across architectures (ViT-L-14, ViT-B-32), we find consistent textual concepts emerging from similar singular vectors for the same tasks. For instance, the singular vectors for both ViT-L-14 at layer 21 and ViT-B-32 at layer 10 align with almost equal phrases. This consistency hints at the intriguing possibility of transferring semantic information across architectures using text embeddings as an interpretable common ground.

We further note that the interpretability of these embeddings strongly depends on the chosen routing layer. While mid-to-late layers (e.g., layer 10 in ViT-B-32 and layer 21 in ViT-L-14) yield semantically meaningful descriptions aligned closely with each dataset’s visual domain, earlier layers (e.g., layer 3 in ViT-B-32) produce irrelevant or misleading concepts such as “IMAGE WITH A PENGUIN” for the texture dataset (DTD) or “PHOTO TAKEN IN SAN-

TORINI, GREECE” for digit classification (MNIST). Such discrepancies suggest that early layers encode generic or low-level visual features, while mid-to-late layers become progressively specialized toward domain-specific semantic structures.

Overall, these analyses validate our routing strategy: the task singular vectors at mid-layer embeddings capture precisely the semantic differences the router exploits to discriminate tasks.

Batched inference

In the main experiments, we evaluated our method in the most challenging scenario, where each sample may belong to a different task, forcing the router to operate per input. Yet, in many practical settings (e.g., batched requests from the same domain), several inputs share the same task. In such cases, we can router-select a single merged model once per batch, closing the gap almost entirely: as shown in Figure 6, our approach achieves a mean normalized accuracy of at least 0.98 in 8 out of 9 settings, effectively matching individually fine-tuned models. This indicates that while our per-sample approach is already effective, batching can further reduce overhead and boost accuracy.

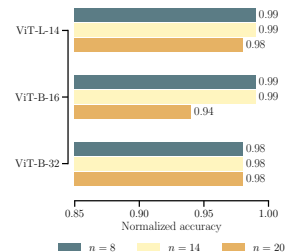


Figure 6. Accuracy in a batched inference scenario.

5. Related Work

Model Merging has recently gained traction as a computationally efficient alternative to ensembling. Early meth-

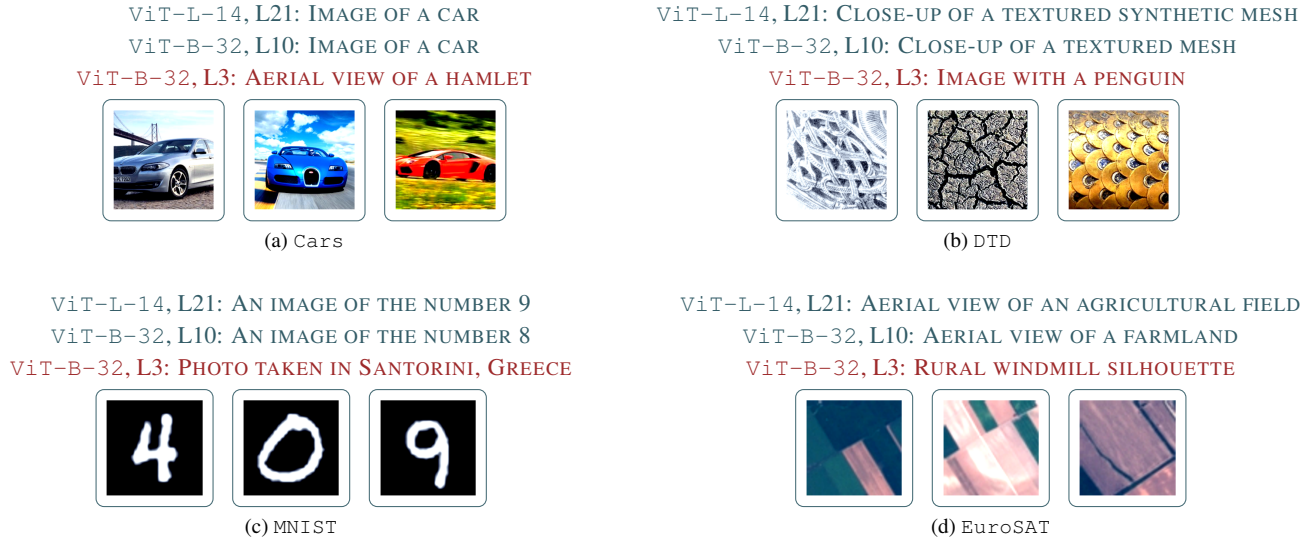


Figure 5. Captions obtained by decoding task singular vectors as text as described in Sec. 4.3, accompanied by task representative images. Captions produced by the task singular vectors of predictive layers reflect the task content, those obtained by non-predictive ones do not.

ods, motivated by linear mode connectivity [21, 23, 26, 43], primarily aligned models trained with different optimization seeds. This was achieved by finding neuron permutations matching these ones before the aggregation [1, 13, 28, 31, 36, 45, 54, 57]. More recent merging approaches aggregate instead multiple fine-tuned models derived from a shared pretrained backbone [14, 16, 25, 33, 34, 41, 42, 48, 58, 61, 65, 66, 69, 71, 74, 76]. These methods incorporate various strategies to improve the merging, such as finding the optimal combination of task vectors [72], mitigating sign disagreement [69], randomly dropping a fraction of the updates [74], or employing evolutionary strategies [2, 42]. The most recent line of work considers task vectors at a layer level, accounting this way for the natural structure of the layers and significantly improving the merging outcome [15, 25, 58]. Our approach builds upon the latter methodologies by introducing adaptivity through input-driven routing, significantly narrowing the performance gap between the finetuned endpoints and their resulting merge.

Model Merging with Mixture-of-Experts, often referred to as “MoErging” [4, 6, 8, 29, 35, 40, 44, 49, 59, 62, 63, 70, 75], explores how independently trained experts—potentially contributed by a decentralized community—can be combined within a single adaptive model by dynamically selecting which expert(s) should handle a given input. In the LLM domain, specialized modules (e.g., LoRAs or adapters) are merged via parametric or data-driven routers that match the incoming prompt to the most relevant module [4, 6, 8, 35, 44, 49, 63, 75]; some approaches, such as PHATGOOSE [44], require fine-tuning additional routing parameters, whereas others, like weight-ensembling

MoE [63], may need to train the router at test time. Sharing a similar two-pass pipeline, *Transformer*² [59] modifies the finetuning procedure to yield task-aligned singular vectors, allowing for expert routing at test time. Differently from the latter, MASS works on any independently finetuned models finetuned with no ad hoc routines. A similar strategy was independently introduced by SMILE [62], which—like our method—enables data-free merging of multiple experts. However, SMILE leaves the pretrained backbone intact and selectively *adds* task-specific low-rank updates at inference, whereas MASS begins with a single model containing all updates and *deactivates* any irrelevant subspaces via a router. The fact that both lines of work arrived at a similar subspace-activation concept, despite differing motivations, highlights the versatility and broad appeal of such an approach. Lastly, *TwinMerging* [40] similarly merges a shared expert and multiple task-specific experts via a gating function. However, *TwinMerging* relies on flat task arithmetic [34] and requires per-task labeled data to train its router, reducing its applicability. In contrast, MASS operates in a fully data-free and training-free regime by design.

6. Conclusions

In this paper, we introduced MASS (MoErging through Adaptive Subspace Selection), a new MoErging approach that leverages low-rank task updates while adaptively routing each input to the most relevant subspace. Given the lack of access to per-task datasets in real-world merging scenarios, we coupled MASS with a projection-based router that operates entirely training- and data-free.

Our extensive experiments show MASS establishing

new state-of-the-art results, recovering nearly the full accuracy of individual task-specific models at a fraction of their combined storage cost. Looking ahead, promising directions include further refining the router for more granular subspace selection and adapting MASS to out-of-distribution scenarios, where different singular vectors can be combined on the fly to solve new unseen tasks.

7. Acknowledgments

This work was partially supported by PRIN 2022 project 20227YET9B “AdVVent” CUP code B53D23012830006 and by projects FAIR (PE0000013) and SERICS (PE0000014) under the MUR National Recovery and Resilience Plan funded by the European Union - NextGenerationEU. This work was moreover partially supported by the project NEREO (Neural Reasoning over Open Data) project funded by the Italian Ministry of Education and Research (PRIN) Grant no. 2022AEFHAZ. We finally acknowledge ISCRA for awarding this project access to the LEONARDO supercomputer, owned by the EuroHPC Joint Undertaking, hosted by CINECA (Italy).

References

- [1] Samuel K. Ainsworth, Jonathan Hayase, and Siddhartha S. Srinivasa. Git re-basin: Merging models modulo permutation symmetries. In *The Eleventh International Conference on Learning Representations, ICLR 2023, Kigali, Rwanda, May 1-5, 2023*, 2023. 1, 8
- [2] Takuya Akiba, Makoto Shing, Yujin Tang, Qi Sun, and David Ha. Evolutionary optimization of model merging recipes. *Nature Machine Intelligence*, 2025. 1, 8
- [3] Lorenzo Basile, Valentino Maiorca, Luca Bortolussi, Emanuele Rodolà, and Francesco Locatello. Residual transformer alignment with spectral decomposition. *arXiv preprint arXiv:2411.00246*, 2024. 7
- [4] Joshua Belofsky. Token-level adaptation of lora adapters for downstream task generalization. In *Proceedings of the 2023 6th Artificial Intelligence and Cloud Computing Conference*, pages 168–172, 2023. 8
- [5] Lukas Bossard, Matthieu Guillaumin, and Luc Van Gool. Food-101 – Mining Discriminative Components with Random Forests. In *Computer Vision – ECCV 2014*, pages 446–461, Cham, 2014. Springer International Publishing. 5, 1
- [6] Feng Cheng, Ziyang Wang, Yi-Lin Sung, Yan-Bo Lin, Mohit Bansal, and Gedas Bertasius. Dam: Dynamic adapter merging for continual video qa learning. *arXiv preprint arXiv:2403.08755*, 2024. 8
- [7] Gong Cheng, Junwei Han, and Xiaoqiang Lu. Remote Sensing Image Scene Classification: Benchmark and State of the Art. *Proceedings of the IEEE*, 105(10):1865–1883, 2017. Conference Name: Proceedings of the IEEE. 5, 1
- [8] Alexandra Chronopoulou, Matthew E Peters, Alexander Fraser, and Jesse Dodge. Adaptersoup: Weight averaging to improve generalization of pretrained language models. *arXiv preprint arXiv:2302.07027*, 2023. 8
- [9] Mircea Cimpoi, Subhransu Maji, Iasonas Kokkinos, Sammy Mohamed, and Andrea Vedaldi. Describing Textures in the Wild. In *2014 IEEE Conference on Computer Vision and Pattern Recognition*, pages 3606–3613, Columbus, OH, USA, 2014. IEEE. 5, 7, 1
- [10] Tarin Clanuwat, Mikel Bober-Irizar, Asanobu Kitamoto, Alex Lamb, Kazuaki Yamamoto, and David Ha. Deep Learning for Classical Japanese Literature, 2018. arXiv:1812.01718 [cs, stat]. 5, 1
- [11] Adam Coates, Andrew Ng, and Honglak Lee. An Analysis of Single-Layer Networks in Unsupervised Feature Learning. In *Proceedings of the Fourteenth International Conference on Artificial Intelligence and Statistics*, pages 215–223. JMLR Workshop and Conference Proceedings, 2011. ISSN: 1938-7228. 5, 1
- [12] Gregory Cohen, Saeed Afshar, Jonathan Tapson, and André van Schaik. EMNIST: Extending MNIST to handwritten letters. In *2017 International Joint Conference on Neural Networks (IJCNN)*, pages 2921–2926, 2017. ISSN: 2161-4407. 5, 1
- [13] Donato Crisostomi, Marco Fumero, Daniele Baieri, Florian Bernard, and Emanuele Rodolà. C²M³: Cycle-consistent multi-model merging. In *Advances in Neural Information Processing Systems*, 2025. 1, 8
- [14] Nico Daheim, Thomas Möllenhoff, Edoardo Ponti, Iryna Gurevych, and Mohammad Emtiyaz Khan. Model merging by uncertainty-based gradient matching. In *The Twelfth International Conference on Learning Representations*. 1, 8
- [15] Marczak Daniel, Magistri Simone, Cygert Sebastian, Twardowski Bartłomiej, D Bagdanov Andrew, and Joost van de Weijer. No task left behind: Isotropic model merging with common and task-specific subspaces. *ArXiv preprint*, 2025. 2, 5, 8
- [16] MohammadReza Davari and Eugene Belilovsky. Model breadcrumbs: Scaling multi-task model merging with sparse masks. In *European Conference on Computer Vision*. Springer, 2025. 8
- [17] Jacob Devlin, Ming-Wei Chang, Kenton Lee, and Kristina Toutanova. Bert: Pre-training of deep bidirectional transformers for language understanding. In *Proceedings of the 2019 conference of the North American chapter of the association for computational linguistics: human language technologies, volume 1 (long and short papers)*, pages 4171–4186, 2019. 1
- [18] Alexey Dosovitskiy, Lucas Beyer, Alexander Kolesnikov, Dirk Weissenborn, Xiaohua Zhai, Thomas Unterthiner, Mostafa Dehghani, Matthias Minderer, Georg Heigold, Sylvain Gelly, Jakob Uszkoreit, and Neil Houlsby. An image is worth 16x16 words: Transformers for image recognition at scale, 2021. 4
- [19] Nan Du, Yanping Huang, Andrew M Dai, Simon Tong, Dmitry Lepikhin, Yuanzhong Xu, Maxim Krikun, Yanqi Zhou, Adams Wei Yu, Orhan Firat, et al. Glam: Efficient scaling of language models with mixture-of-experts. In *International conference on machine learning*, pages 5547–5569. PMLR, 2022. 2
- [20] David Eigen, Marc’Aurelio Ranzato, and Ilya Sutskever.

- Learning factored representations in a deep mixture of experts, 2014. 2
- [21] Rahim Entezari, Hanie Sedghi, Olga Saukh, and Behnam Neyshabur. The role of permutation invariance in linear mode connectivity of neural networks. In *The Tenth International Conference on Learning Representations, ICLR 2022, Virtual Event, April 25-29, 2022*, 2022. 8
- [22] William Fedus, Barret Zoph, and Noam Shazeer. Switch transformers: Scaling to trillion parameter models with simple and efficient sparsity. *Journal of Machine Learning Research*, 23(120):1–39, 2022. 2
- [23] Jonathan Frankle, Gintare Karolina Dziugaite, Daniel Roy, and Michael Carbin. Linear mode connectivity and the lottery ticket hypothesis. In *Proceedings of the 37th International Conference on Machine Learning, ICML 2020, 13-18 July 2020, Virtual Event, 2020*. 8
- [24] Yossi Gandelsman, Alexei A Efros, and Jacob Steinhardt. Interpreting clip’s image representation via text-based decomposition. In *ICLR*, 2024. 7
- [25] Antonio Andrea Gargiulo, Donato Crisostomi, Maria Sofia Bucarelli, Simone Scardapane, Fabrizio Silvestri, and Emanuele Rodolà. Task singular vectors: Reducing task interference in model merging. In *Proc. CVPR*, 2025. 1, 2, 3, 4, 5, 8
- [26] Timur Garipov, Pavel Izmailov, Dmitrii Podoprikin, Dmitry P. Vetrov, and Andrew Gordon Wilson. Loss surfaces, mode connectivity, and fast ensembling of dnns. In *Advances in Neural Information Processing Systems 31: Annual Conference on Neural Information Processing Systems 2018, NeurIPS 2018, December 3-8, 2018, Montréal, Canada*, 2018. 8
- [27] Ian J. Goodfellow, Dumitru Erhan, Pierre Luc Carrier, Aaron Courville, Mehdi Mirza, Ben Hamner, Will Cukierski, Yichuan Tang, David Thaler, Dong-Hyun Lee, Yingbo Zhou, Chetan Ramaiah, Fangxiang Feng, Ruifan Li, Xiaojie Wang, Dimitris Athanasakis, John Shawe-Taylor, Maxim Milakov, John Park, Radu Ionescu, Marius Popescu, Cristian Grozea, James Bergstra, Jingjing Xie, Lukasz Romaszko, Bing Xu, Zhang Chuang, and Yoshua Bengio. Challenges in Representation Learning: A Report on Three Machine Learning Contests. In *Neural Information Processing*, pages 117–124, Berlin, Heidelberg, 2013. Springer. 5, 1
- [28] Fidel A. Guerrero-Peña, Heitor Rapela Medeiros, Thomas Dubail, Masih Aminbeidokhti, Eric Granger, and Marco Pedersoli. Re-basin via implicit sinkhorn differentiation. In *IEEE/CVF Conference on Computer Vision and Pattern Recognition, CVPR 2023, Vancouver, BC, Canada, June 17-24, 2023*, 2023. 8
- [29] Shwai He, Run-Ze Fan, Liang Ding, Li Shen, Tianyi Zhou, and Dacheng Tao. Merging experts into one: Improving computational efficiency of mixture of experts. In *Proceedings of the 2023 Conference on Empirical Methods in Natural Language Processing*, pages 14685–14691, 2023. 8
- [30] Patrick Helber, Benjamin Bischke, Andreas Dengel, and Damian Borth. EuroSAT: A Novel Dataset and Deep Learning Benchmark for Land Use and Land Cover Classification. *IEEE Journal of Selected Topics in Applied Earth Observations and Remote Sensing*, 12(7):2217–2226, 2019. Conference Name: IEEE Journal of Selected Topics in Applied Earth Observations and Remote Sensing. 5, 1
- [31] Stefan Horoi, Albert Manuel Orozco Camacho, Eugene Belilovsky, and Guy Wolf. Harmony in Diversity: Merging Neural Networks with Canonical Correlation Analysis. 2024. 8
- [32] Edward J Hu, Yelong Shen, Phillip Wallis, Zeyuan Allen-Zhu, Yuanzhi Li, Shean Wang, Lu Wang, Weizhu Chen, et al. Lora: Low-rank adaptation of large language models. *ICLR*, 1(2):3, 2022. 1
- [33] Chenyu Huang, Peng Ye, Tao Chen, Tong He, Xiangyu Yue, and Wanli Ouyang. Emr-merging: Tuning-free high-performance model merging, 2024. 1, 8
- [34] Gabriel Ilharco, Marco Túlio Ribeiro, Mitchell Wortsman, Ludwig Schmidt, Hannaneh Hajishirzi, and Ali Farhadi. Editing models with task arithmetic. In *The Eleventh International Conference on Learning Representations, ICLR 2023, Kigali, Rwanda, May 1-5, 2023*, 2023. 1, 2, 4, 5, 8
- [35] Joel Jang, Seungone Kim, Seonghyeon Ye, Doyoung Kim, Lajanugen Logeswaran, Moontae Lee, Kyungjae Lee, and Minjoon Seo. Exploring the benefits of training expert language models over instruction tuning. In *International Conference on Machine Learning*, pages 14702–14729. PMLR, 2023. 8
- [36] Keller Jordan, Hanie Sedghi, Olga Saukh, Rahim Entezari, and Behnam Neyshabur. REPAIR: renormalizing permuted activations for interpolation repair. In *The Eleventh International Conference on Learning Representations, ICLR 2023, Kigali, Rwanda, May 1-5, 2023*, 2023. 8
- [37] Jonathan Krause, Michael Stark, Jia Deng, and Li Fei-Fei. 3D Object Representations for Fine-Grained Categorization. In *2013 IEEE International Conference on Computer Vision Workshops*, pages 554–561, Sydney, Australia, 2013. IEEE. 5, 7, 1
- [38] Alex Krizhevsky and Geoffrey Hinton. Learning multiple layers of features from tiny images. Technical Report 0, University of Toronto, Toronto, Ontario, 2009. 5, 1
- [39] Y. Lecun, L. Bottou, Y. Bengio, and P. Haffner. Gradient-based learning applied to document recognition. *Proceedings of the IEEE*, 86(11):2278–2324, 1998. 5, 1
- [40] Zhenyi Lu, Chenghao Fan, Wei Wei, Xiaoye Qu, Dangyang Chen, and Yu Cheng. Twin-merging: Dynamic integration of modular expertise in model merging. In *The Thirty-eighth Annual Conference on Neural Information Processing Systems*, 2024. 2, 5, 8
- [41] Michael Matena and Colin Raffel. Merging models with fisher-weighted averaging. In *Advances in Neural Information Processing Systems 35: Annual Conference on Neural Information Processing Systems 2022, NeurIPS 2022, New Orleans, LA, USA, November 28 - December 9, 2022*, 2022. 8
- [42] Tommaso Mencattini, Adrian Robert Minut, Donato Crisostomi, Andrea Santilli, and Emanuele Rodolà. Merge³: Efficient evolutionary merging on consumer-grade gpus. *arXiv preprint arXiv:2502.10436*, 2025. 8
- [43] Seyed-Iman Mirzadeh, Mehrdad Farajtabar, Dilan Görür, Razvan Pascanu, and Hassan Ghasemzadeh. Linear mode

- connectivity in multitask and continual learning. In *9th International Conference on Learning Representations, ICLR 2021, Virtual Event, Austria, May 3-7, 2021*, 2021. 8
- [44] Mohammed Muqeeth, Haokun Liu, Yufan Liu, and Colin Raffel. Learning to route among specialized experts for zero-shot generalization. In *International Conference on Machine Learning*, pages 36829–36846, 2024. 8
- [45] Aviv Navon, Aviv Shamsian, Ethan Fetaya, Gal Chechik, Nadav Dym, and Haggai Maron. Equivariant deep weight space alignment, 2023. 8
- [46] Yuval Netzer, Tao Wang, Adam Coates, Alessandro Bis-sacco, Bo Wu, and Andrew Y. Ng. Reading digits in natural images with unsupervised feature learning. In *NIPS Workshop on Deep Learning and Unsupervised Feature Learning 2011*, 2011. 5, 1
- [47] Maria-Elena Nilsback and Andrew Zisserman. Automated Flower Classification over a Large Number of Classes. In *2008 Sixth Indian Conference on Computer Vision, Graphics & Image Processing*, pages 722–729, 2008. 5, 1
- [48] Guillermo Ortiz-Jiménez, Alessandro Favero, and Pascal Frossard. Task arithmetic in the tangent space: Improved editing of pre-trained models. In *Advances in Neural Information Processing Systems 36: Annual Conference on Neural Information Processing Systems 2023, NeurIPS 2023, New Orleans, LA, USA, December 10 - 16, 2023*, 2023. 1, 8
- [49] Oleksiy Ostapenko, Zhan Su, Edoardo Maria Ponti, Laurent Charlin, Nicolas Le Roux, Matheus Pereira, Lucas Caccia, and Alessandro Sordani. Towards modular llms by building and reusing a library of lorae. *arXiv preprint arXiv:2405.11157*, 2024. 8
- [50] Omkar M Parkhi, Andrea Vedaldi, Andrew Zisserman, and C. V. Jawahar. Cats and dogs. In *2012 IEEE Conference on Computer Vision and Pattern Recognition*, pages 3498–3505, 2012. ISSN: 1063-6919. 5, 1
- [51] Jonas Pfeiffer, Aishwarya Kamath, Andreas Rücklé, Kyunghyun Cho, and Iryna Gurevych. Adapterfusion: Non-destructive task composition for transfer learning. In *Proceedings of the 16th Conference of the European Chapter of the Association for Computational Linguistics: Main Volume*, pages 487–503, 2021. 2
- [52] Alec Radford, Jong Wook Kim, Chris Hallacy, Aditya Ramesh, Gabriel Goh, Sandhini Agarwal, Girish Sastry, Amanda Askell, Pamela Mishkin, Jack Clark, et al. Learning transferable visual models from natural language supervision. In *International conference on machine learning*, pages 8748–8763. PMLR, 2021. 1, 4
- [53] Noam Shazeer, Azalia Mirhoseini, Krzysztof Maziarz, Andy Davis, Quoc Le, Geoffrey Hinton, and Jeff Dean. Outrageously large neural networks: The sparsely-gated mixture-of-experts layer, 2017. 2
- [54] Sidak Pal Singh and Martin Jaggi. Model fusion via optimal transport. In *Advances in Neural Information Processing Systems 33: Annual Conference on Neural Information Processing Systems 2020, NeurIPS 2020, December 6-12, 2020, virtual*, 2020. 1, 8
- [55] Richard Socher, Alex Perelygin, Jean Wu, Jason Chuang, Christopher D. Manning, Andrew Ng, and Christopher Potts. Recursive deep models for semantic compositionality over a sentiment treebank. In *Proceedings of the 2013 Conference on Empirical Methods in Natural Language Processing*, pages 1631–1642, Seattle, Washington, USA, 2013. Association for Computational Linguistics. 5, 1
- [56] Johannes Stalkamp, Marc Schlipf, Jan Salmen, and Christian Igel. The German Traffic Sign Recognition Benchmark: A multi-class classification competition. In *The 2011 International Joint Conference on Neural Networks*, pages 1453–1460, 2011. ISSN: 2161-4407. 5, 1
- [57] George Stoica, Daniel Bolya, Jakob Brandt Björner, Pratik Ramesh, Taylor Hearn, and Judy Hoffman. Zipit! merging models from different tasks without training. In *The Twelfth International Conference on Learning Representations*, . 8
- [58] George Stoica, Pratik Ramesh, Boglarka Ecsedi, Leshem Choshen, and Judy Hoffman. Model merging with svd to tie the knots. In *The Thirteenth International Conference on Learning Representations*, . 8
- [59] Qi Sun, Edoardo Cetin, and Yujin Tang. Transformer-squared: Self-adaptive llms. In *The Thirteenth International Conference on Learning Representations*, 2025. 8
- [60] Chuanqi Tan, Fuchun Sun, Tao Kong, Wenchang Zhang, Chao Yang, and Chunfang Liu. A survey on deep transfer learning. In *Artificial Neural Networks and Machine Learning–ICANN 2018: 27th International Conference on Artificial Neural Networks, Rhodes, Greece, October 4-7, 2018, Proceedings, Part III 27*, pages 270–279. Springer, 2018. 1
- [61] Anke Tang, Li Shen, Yong Luo, Yibing Zhan, Han Hu, Bo Du, Yixin Chen, and Dacheng Tao. Parameter-efficient multi-task model fusion with partial linearization. In *The Twelfth International Conference on Learning Representations*. 8
- [62] Anke Tang, Li Shen, Yong Luo, Shuai Xie, Han Hu, Lefei Zhang, Bo Du, and Dacheng Tao. Smile: Zero-shot sparse mixture of low-rank experts construction from pre-trained foundation models. *arXiv preprint arXiv:2408.10174*, 2024. 8
- [63] Anke Tang, Li Shen, Yong Luo, Nan Yin, Lefei Zhang, and Dacheng Tao. Merging multi-task models via weight-ensembling mixture of experts. In *International Conference on Machine Learning*, pages 47778–47799. PMLR, 2024. 2, 8
- [64] Bastiaan S. Veeling, Jasper Linmans, Jim Winkens, Taco Cohen, and Max Welling. Rotation Equivariant CNNs for Digital Pathology. In *Medical Image Computing and Computer Assisted Intervention – MICCAI 2018*, pages 210–218, Cham, 2018. Springer International Publishing. 5, 1
- [65] Ke Wang, Nikolaos Dimitriadis, Guillermo Ortiz-Jimenez, François Fleuret, and Pascal Frossard. Localizing task information for improved model merging and compression. In *Proceedings of the 41st International Conference on Machine Learning*, 2024. 1, 4, 5, 8
- [66] Mitchell Wortsman, Gabriel Ilharco, Jong Wook Kim, Mike Li, Simon Kornblith, Rebecca Roelofs, Raphael Gontijo-Lopes, Hannaneh Hajishirzi, Ali Farhadi, Hongseok Namkoong, and Ludwig Schmidt. Robust fine-tuning of zero-shot models, 2021. 8

- [67] Han Xiao, Kashif Rasul, and Roland Vollgraf. Fashion-MNIST: a Novel Image Dataset for Benchmarking Machine Learning Algorithms, 2017. arXiv:1708.07747 [cs, stat]. 5, 1
- [68] Jianxiong Xiao, Krista A. Ehinger, James Hays, Antonio Torralba, and Aude Oliva. SUN Database: Exploring a Large Collection of Scene Categories. *International Journal of Computer Vision*, 119(1):3–22, 2016. 5, 1
- [69] Prateek Yadav, Derek Tam, Leshem Choshen, Colin A. Raffel, and Mohit Bansal. Ties-merging: Resolving interference when merging models. In *Advances in Neural Information Processing Systems 36: Annual Conference on Neural Information Processing Systems 2023, NeurIPS 2023, New Orleans, LA, USA, December 10 - 16, 2023*, 2023. 1, 8
- [70] Prateek Yadav, Colin Raffel, Mohammed Muqeeth, Lucas Caccia, Haokun Liu, Tianlong Chen, Mohit Bansal, Leshem Choshen, and Alessandro Sordoni. A survey on model merging: Recycling and routing among specialized experts for collaborative learning, 2024. 2, 8
- [71] Enneng Yang, Li Shen, Zhenyi Wang, Guibing Guo, Xiaojun Chen, Xingwei Wang, and Dacheng Tao. Representation surgery for multi-task model merging. In *Proceedings of the 41st International Conference on Machine Learning*, 2024. 8
- [72] Enneng Yang, Zhenyi Wang, Li Shen, Shiwei Liu, Guibing Guo, Xingwei Wang, and Dacheng Tao. Adamerging: Adaptive model merging for multi-task learning. In *The Twelfth International Conference on Learning Representations*, 2024. 8
- [73] Jason Yosinski, Jeff Clune, Yoshua Bengio, and Hod Lipson. How transferable are features in deep neural networks? *Advances in neural information processing systems*, 27, 2014. 1
- [74] Le Yu, Bowen Yu, Haiyang Yu, Fei Huang, and Yongbin Li. Language models are super mario: Absorbing abilities from homologous models as a free lunch. In *Proceedings of the 41st International Conference on Machine Learning*, 2024. 1, 8
- [75] Ziyu Zhao, Leilei Gan, Guoyin Wang, Wangchunshu Zhou, Hongxia Yang, Kun Kuang, and Fei Wu. Loraretriever: Input-aware lora retrieval and composition for mixed tasks in the wild. *arXiv preprint arXiv:2402.09997*, 2024. 8
- [76] Luca Zhou, Daniele Solombrino, Donato Crisostomi, Maria Sofia Bucarelli, Fabrizio Silvestri, and Emanuele Rodolà. Atm: Improving model merging by alternating tuning and merging, 2024. 1, 8

MASS: MoErting through Adaptive Subspace Selection

Supplementary Material

8. Additional details

We here describe the details required to implement and reproduce our results. The code is provided in the supplementary materials. In particular, Sec. 8.1 describes implementation details, Sec. 8.2 specifies the employed evaluation metrics, Sec. 8.3 reports the employed architecture and Sec. 8.4 specifies the hyperparameters and how they were chosen.

8.1. Implementation

We used the same model checkpoints as `Consensus TA` [65], except for the one for the `EMNIST` dataset which we had to re-finetune due to an inconsistency in image orientation between `EMNIST` and `MNIST`. Shortly, the `torchvision`³ version yields rotated and flipped images, spuriously yielding extremely similar models (same classes, roughly same dataset statistics) that performed very poorly when interchanged. Simply re-rotating and flipping the `EMNIST` images to match the orientation of `MNIST` solves the issue. We further used a single classification head for `STL10` and `CIFAR10` due to their 9 shared classes. The final head has the shared classes plus the two dataset-specific ones, *i.e.* monkey and frog.

8.2. Evaluation measures

To account for differences in task difficulty, we report both *absolute* and *normalized* accuracy in our results. The normalized accuracy serves as a relative performance measure by comparing the multi-task model’s accuracy to that of individual fine-tuned models. It is computed as:

$$\text{Normalized Accuracy} = \frac{1}{T} \sum_{i=1}^T \frac{\text{accuracy}(\theta_{MT}, t_i)}{\text{accuracy}(\theta_{ft_i}, t_i)} \quad (7)$$

where T represents the total number of tasks, θ_{MT} is the multi-task model, and θ_{ft_i} corresponds to the fine-tuned model for task t_i . By normalizing accuracy in this way, we ensure a fairer comparison that accounts for variations in baseline task performance.

8.3. Architectures

We use CLIP from the `OpenClip` library⁴, using the three different versions described in Tab. 5. For the router, we use a small two-layer MLP with a hidden dimension of 1024. It accepts a 512-dimensional embedding vector, applies a linear transformation, a ReLU activation, and dropout with a probability of 0.5, and outputs logits corresponding to task selection probabilities.

³<https://pytorch.org/vision/stable/index.html>

⁴https://github.com/mlfoundations/open_clip/

Dataset	image size	# train	# val	# test
Cars [37]	varies	7330	814	8041
DTD [9]	varies	1692	188	1880
EuroSAT [30]	64 × 64	21600	2700	2700
GTSRB [56]	varies	23976	2664	12630
MNIST [39]	28 × 28	55000	5000	10000
RESISC45 [7]	256 × 256	17010	1890	6300
SUN397 [68]	varies	17865	1985	19850
SVHN [46]	32 × 32	68257	5000	26032
CIFAR100 [38]	32 × 32	45000	5000	10000
STL10 [11]	96 × 96	4500	500	8000
Flowers102 [47]	varies	918	102	6149
OxfordIIITPet [50]	varies	3312	368	3669
PCAM [64]	96 × 96	257144	5000	32768
FER2013 [27]	48 × 48	25839	2870	7178
EMNIST [12]	28 × 28	235000	5000	40000
CIFAR10 [38]	32 × 32	45000	5000	10000
Food101 [5]	512 × 512	70750	5000	25250
FashionMNIST [67]	28 × 28	55000	5000	10000
RenderedSST2 [55]	varies	6228	692	1821
KMNIST [10]	28 × 28	55000	5000	10000

Table 4. Image sizes, and numbers of train, validation, and test samples for the considered datasets.

Model	Layers	Hidden Dim	Heads	Patch Size	Params
ViT-B-32	12	768	12	32×32	~86M
ViT-B-16	12	768	12	16×16	~86M
ViT-L-14	24	1024	16	14×14	~307M

Table 5. Comparison of ViT-B-32, ViT-B-16, and ViT-L-14 architectures.

8.4. Hyperparameter Settings

Following the recommendation of TSV [25], we use α as a single scaling factor with the suggested value of 1.0 for the TSV-M merging configurations in both Algorithm 1 and Algorithm 2. Consistent with TSV, the compression rate assigned to each task space is set to $\frac{1}{T}$. We optimized the similarity threshold ε over the range $\{0.1, 0.2, \dots, 0.9\}$ and determine the router’s selection threshold η via a Bayesian search within the interval $[0.05, 0.5]$. As illustrated in Fig-

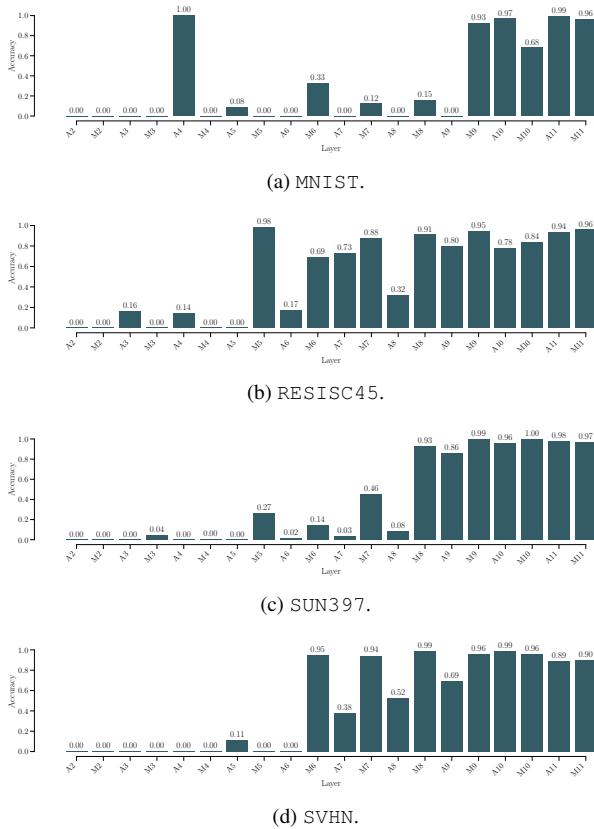


Figure 7. Per-layer task accuracies for ViT-B-32 on MNIST, RESISC45, SUN397, and SVHN.

ures 3a, 3b and 11, we identify the optimal projection layer by focusing on those revealing the highest task accuracy. Specifically, for ViT-B-32 and ViT-B-16 models, we select the attention and MLP layers within the range $\{7, \dots, 11\}$, while for the ViT-L-14 model, the chosen layers fall in the range $\{19, \dots, 23\}$. The temperature parameter for tuning the behavior of the softmax function at line 6 in Algorithm 2 is set to 1.

9. Additional experiments and results

In this section, we provide detailed per-task and per-layer accuracy plots, along with further examples of decoded task vectors, to complement the results presented in the main paper.

Radars charts on 8- and 14-task benchmarks. In section Section 4, we present comprehensive results for the approach using the 20 task benchmark. Figure 9 and Figure 10 respectively display the normalized accuracies for our method on 8 and 14 tasks across all three model sizes (ViT-B-32, ViT-B-16, and ViT-L-14). In both cases, the approach retains a high fraction of each fine-

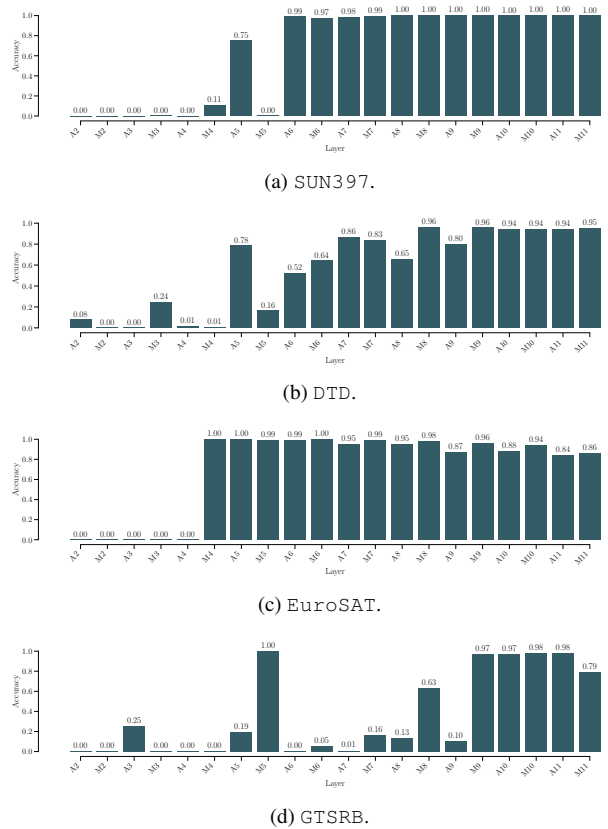


Figure 8. Per-layer task accuracies for ViT-B-32 on Cars, DTD, EuroSAT, and GTSRB.

tuned model’s performance, with normalized accuracies often above 80–90%. Notably, the method scales gracefully as the number of tasks increases from 8 to 14.

Layer-wise accuracies for individual datasets. Figures 8 and 7 show per-layer accuracies for ViT-B-32 on different subsets of the 8-task benchmark:

- Figure 8 focuses on Cars, DTD, EuroSAT, and GTSRB.
- Figure 7 displays results for MNIST, RESISC45, SUN397, and SVHN.

Again, the top-performing layer is not shared across the tasks, confirming what we observed in the main paper.

Layer-wise accuracies for ViT-L-14. Figure 11 reports average per-layer task accuracy for the larger ViT-L-14, showing that in this case the most predictive layer for routing is $\ell = 20$. Since ViT-L-14 has 24 layers (compared to the 12 layers in ViT-B-32 and ViT-B-16), the most predictive layer is roughly at the same relative depth.

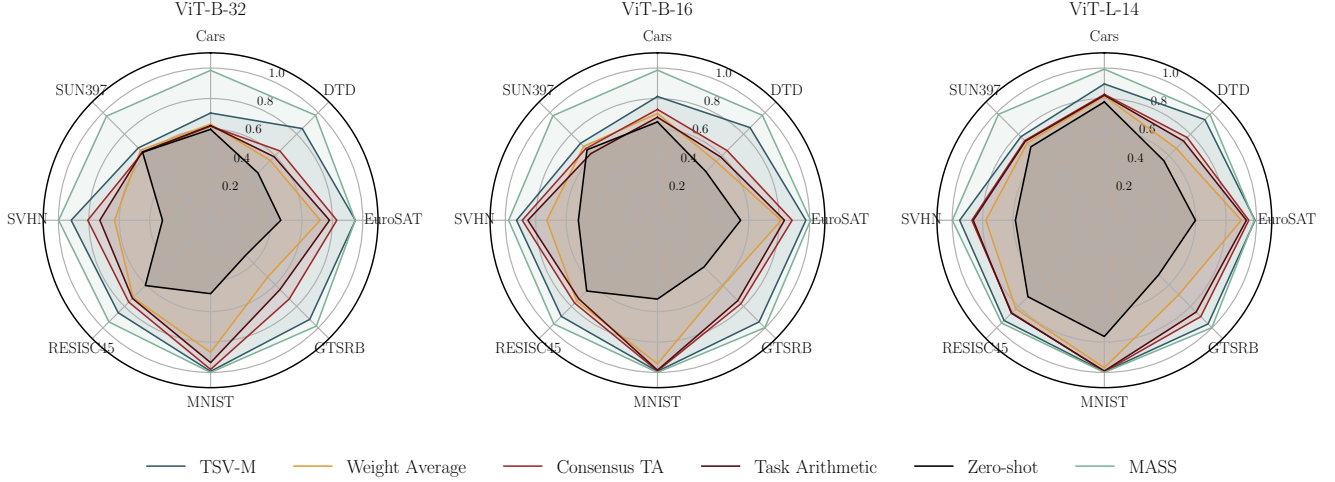


Figure 9. Normalized task accuracies over models ViT-B-32, ViT-B-16 and ViT-L-14 for the 8 tasks benchmark.

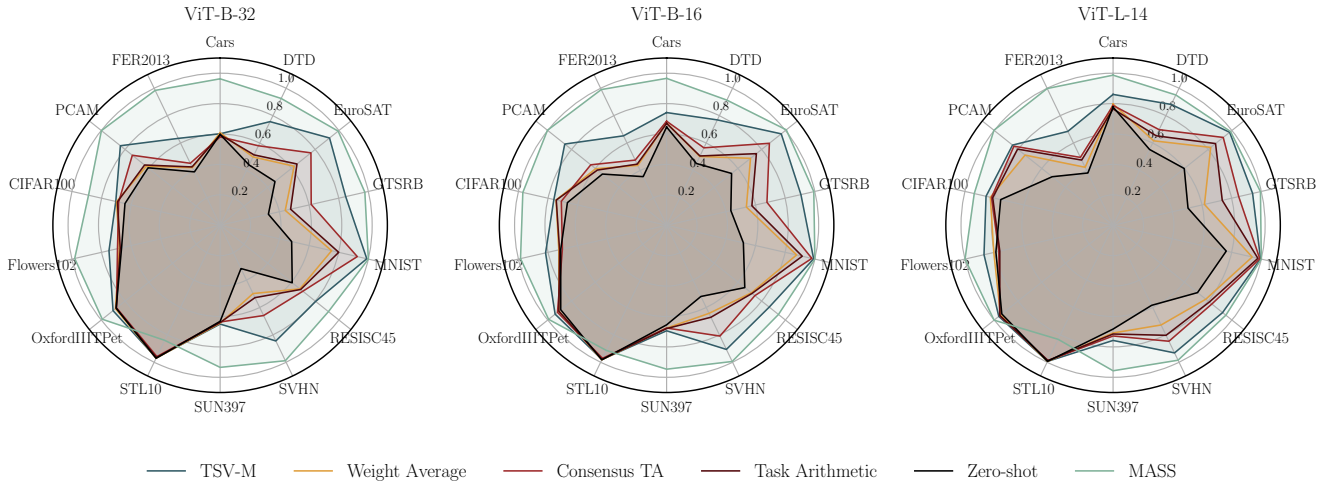


Figure 10. Normalized task accuracies over models ViT-B-32, ViT-B-16 and ViT-L-14 for the 14 tasks benchmark.

Visualizations for additional datasets. Following the approach in Sec. 4.3, Figure 12 shows examples of decoded task vectors for datasets like SVHN, GTSRB, SUN397, and RESISC45. Here, we see textual prompts such as “An image of the number 4” or “Aerial view of an industrial area”, which align with each dataset’s distinct domain. This reaffirms that our singular vectors capture domain-specific transformations while preserving high-level semantic alignment to the pretrained model.

10. Mathematical proofs

Proposition 10.1 (Optimality of Orthogonal Projection). *Let $V \in \mathbb{R}^{d \times k}$ have orthonormal columns spanning a subspace $\mathcal{S} \subseteq \mathbb{R}^d$, and let $\mathbf{a} \in \mathbb{R}^d$. Then the unique minimizer*

of $\|\mathbf{a} - \mathbf{w}\|_2^2$ over all $\mathbf{w} \in \mathcal{S}$ is

$$\hat{\mathbf{w}} = V V^\top \mathbf{a}.$$

Proof. Any $\mathbf{w} \in \mathcal{S}$ can be written as $V \boldsymbol{\alpha}$ for some $\boldsymbol{\alpha} \in \mathbb{R}^k$. The problem

$$\min_{\mathbf{w} \in \mathcal{S}} \|\mathbf{a} - \mathbf{w}\|_2^2 \iff \min_{\boldsymbol{\alpha} \in \mathbb{R}^k} \|\mathbf{a} - V \boldsymbol{\alpha}\|_2^2$$

has a strictly convex objective, so its global minimizer is found by setting the gradient to zero. A short calculation shows

$$\boldsymbol{\alpha} = V^\top \mathbf{a} \implies \hat{\mathbf{w}} = V (V^\top \mathbf{a}) = V V^\top \mathbf{a}.$$

Uniqueness follows from the strict convexity, and $\|\mathbf{a} - \hat{\mathbf{w}}\|_2$ is necessarily the smallest possible distance in \mathcal{S} . Equivalently, $\mathbf{a} - \hat{\mathbf{w}}$ is orthogonal to \mathcal{S} , so no further reduction in norm is possible. \square

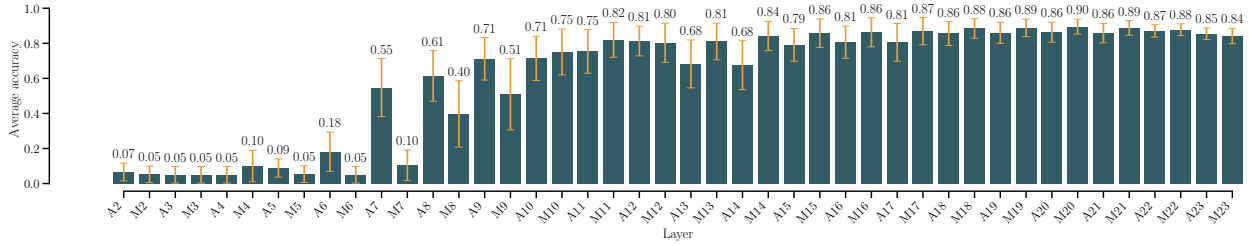


Figure 11. ViT-L-14 per-layer task accuracies.



Figure 12. Captions obtained by decoding task singular vectors as text for datasets SVHN, GTSRB, SUN397, and RESISC45 as described in Sec. 4.3, accompanied by three representative images for each dataset.